Phase Field Modeling of Crack Propagation in Concrete Composite with Imperfect Interface

Gia-Khuyen Le
Campus in Ho Chi Minh City, University of Transport and Communications, Vietnam
khuyenlg_ph@utc.edu.vn

Hoang-Quan Nguyen
University of Transport and Communications, Vietnam
quannh_ktxd@utc.edu.vn (corresponding author)

Tien-Dung Nguyen
University of Transport and Communications, Vietnam
nguyen.tiendung@utc.edu.vn

Received: 19 May 2024 | Revised: 28 May 2024 | Accepted: 29 May 2024

 DOI: https://doi.org/10.48084/etasr.7881

ABSTRACT

In this study, a phase-field model with imperfect interface is developed to simulate the crack behavior of concrete at the mesoscale level. Concrete is treated as a biphasic material, comprising aggregates, a cementitious matrix, and interfaces between them, which are characterized using a level set function. Both cracks and interfaces are represented in a smeared sense by scalar fields ranging from 0 to 1. On the other hand, the displacement jump at the interface is described by an auxiliary field over the entire domain. This model effectively captures the complex crack patterns in concrete, including debonding cracks and bulk cracks. Furthermore, the results show that a strong interface can significantly enhance the mechanical performance of the material.

Keywords-phase field model; smeared crack and interface; level set function; imperfect interface

I. INTRODUCTION

Concrete is a multiphasic material comprising aggregate, mortar matrix, pores, and other weak inclusions, and is widely utilized in engineering structures due to its high compressive strength and durability. Despite these advantages, it has two undesirable properties: low tensile strength and brittleness, making cracking its primary failure mode. As a heterogeneous material, the randomly distributed phases and the interface between them significantly influence crack nucleation location, propagation path, and failure mode, impacting the performance and reliability of structures at the marco scale. In order to improve these negative properties of concrete and propose an optimal design, it is desirable to conduct numerical simulations at the mesoscale level for a deeper understanding of the failure mechanism of this material [1-4]. Due to its heterogeneous nature, concrete exhibits complex crack paths at the mesoscale, including branching, coalescence, bridging, and the competition between interface and bulk cracking. Consequently, simulating crack propagation behavior in concrete poses a challenging task. Various methods are available for modeling crack propagation in solids, which can be broadly categorized into two groups: discrete and smeared methods. In the first group, cracks are treated as discontinuities. Several methods within this category, such as node splitting [5], discrete element modeling [6, 7], and cohesive surfaces [8], have been utilized. However, a drawback of this approach is the strong mesh dependency of the crack path, particularly when remeshing is required. In the second group, cracks are represented as continua through the introduction of reduced material stiffness and/ or strength [9, 10] or via an auxiliary scalar variable [11-13]. Among these methods, the phase field method has recently garnered increasing attention from researchers due to its efficacy in simulating complex crack paths. This approach uses a scalar variable ranging from 0 to 1 to represent the intact and fully broken material. The complex crack paths are effectively and automatically modelled by the evolution of the phases field variable using only a fixed finite element mesh. The tedious task of crack tracking is avoided, presenting a significant advantage over the discrete crack methods.

The interface between phases plays a crucial role in the fracture behavior of heterogeneous materials. Depending on the properties of the interface, there is a competition between bulk cracks and interfacial cracks. Authors in [1] discuss the choice of an appropriate phase field model to describe the fracture behavior of concrete at the mesoscale level by assuming a perfect interface between aggregate and cementitious matrix. Thus, the post-cracking behavior from the numerical model

drops more quickly than observed in experiments. Therefore modeling interfacial cracks using the phase field method remains an ongoing and challenging task. To address this, the cohesive law at the interface must be incorporated into the phase field method. Based on the classic phase field theory, author in [14] proposes a phase-field regularized cohesive-zone model for the cohesive fracture. In this approach, with a special choice of degradation function and the homogeneous energy dissipation function, the phase field method converges to the cohesive zone model. Authors in [15] introduced a cohesive phase field model wherein the displacement jump at the interface is approximated through a smooth transition defined by a level set function and two points near the interface. However, the selection of the location for these two points is somewhat arbitrary and heavily dependent on the specific problem. Authors in [16] proposed a cohesive phase field model that describes the crack and the interface in a smeared manner. Additionally, this approach utilizes an auxiliary field to represent the displacement jump at the interface. This model easily incorporates the cohesive law, contrasting with the phase field model of [9].

In our recent publication [17], we implemented the phase field model with imperfect interface proposed in [16] and conducted an analysis of the accuracy and influence of certain model parameters. This was achieved by comparing the numerical results with the analytical solution of a one-dimensional bar under tension. In this paper, this model is utilized to investigate the failure mechanism of concrete at the mesoscale level, taking into account the influence of the imperfect interface between the aggregates and cement matrix. In this paper, we present the finite element implementation of this model along with two numerical examples are presented to demonstrate the influence of the imperfect interface on the failure mechanism of concrete.

II. PHASE FIELD MODEL WITH IMPERFECT INTERFACE

Let us consider a domain $\Omega \subset \mathcal{R}^{\mathcal{D}}$, with $\mathcal{D} = 1,2,3$, describing a concrete specimen which contain aggregate, matrix and the interface between them. $\partial\Omega \in \mathcal{R}^{D-1}$ represents the external boundary of Ω. Let Γ and Γ^I of dimension $\mathcal{D}-1$ represent the crack and the interface in the domain Ω, respectively. Depending on the characteristics of the interface, the crack may propagate either through the bulk material or along the interface between the matrix and the inclusion. In this work, both the crack and the interface are represented in smeared sense by a scalar phase field $\phi(\boldsymbol{x},t) \in [0,1]$ and a fixed scalar $\alpha(\boldsymbol{x}) \in [0,1]$, respectively (Figure 1).

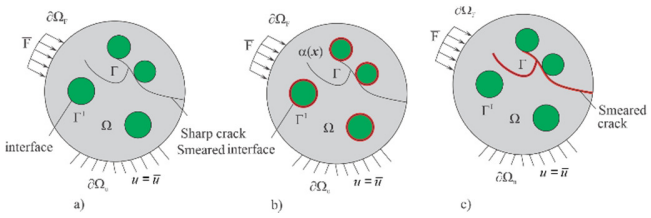

Fig. 1. (a) A domain contain discrete interface and sharp crack, (b) smeared representation of interface (red), (c) smeared representation of crack (red).

A. Phase Field Approximation of Crack and Interface

The phase field distribution $\phi(\boldsymbol{x},\boldsymbol{t})$ and the interface $\alpha(\boldsymbol{x})$ are determined by solving the following variational problem:

$$\begin{aligned} &\phi(\boldsymbol{x}) = Arg\left\{inf_{\phi\in S_\phi}\Gamma_\phi(\phi)\right\}, \\ &\Gamma_\phi(\phi) = \int_\Omega \gamma_\phi\ (\phi,\nabla\phi)d\Omega\ , \\ &S_\phi = \{\phi|\phi(\boldsymbol{x}) = 1\ on\ \Gamma\ \forall \boldsymbol{x}\ \in\ \Gamma\}. \end{aligned} \tag{1}$$

$$\begin{aligned} &\alpha(\boldsymbol{x}) = Arg\{inf_{\alpha\in S_\alpha}\Gamma_\alpha(\alpha)\}, \\ &\Gamma_\alpha(\alpha) = \ \int_\Omega \gamma_\alpha(\alpha,\nabla\alpha)d\Omega\ , \\ &S_\alpha = \{\alpha|\alpha(\boldsymbol{x}) = 1\ \text{on}\ \Gamma_\alpha\ \forall \boldsymbol{x}\ \in\ \Gamma_\alpha\}. \end{aligned} \tag{2}$$

where $\Gamma_\phi(\phi)$ denotes the total crack length and $\Gamma_\alpha(\alpha)$ represents the total interface length. $\gamma_\phi(\phi,\nabla\phi)$ and $\gamma_\alpha(\alpha,\nabla\alpha)$ are the crack density function per unit volume and interface density function per unit volume, respectively. These density functions are defined by:

$$\gamma_\phi(\phi,\nabla\phi) = \frac{1}{2\ell_\phi}\phi^2 + \frac{\ell_\phi}{2}\nabla\phi\cdot\nabla\phi \tag{3}$$

$$\gamma_\alpha(\alpha,\nabla\alpha) = \frac{1}{2\ell_\alpha}\alpha^2 + \frac{\ell_\alpha}{2}\nabla\alpha\cdot\nabla\alpha \tag{4}$$

where ℓ_ϕ, ℓ_α are length scale parameters which represent the widths of regularized crack and interface, respectively. When $\ell_p, \ell_\alpha \to 0$, the smeared crack and interface converge towards the discrete crack and interface.

The boundary problem for the smeared crack is defined as follows:

$$\begin{cases} \phi(\boldsymbol{x}) - \ell_\phi^2\Delta\phi(\boldsymbol{x}) = 0 & (\Omega) \\ \phi(\boldsymbol{x}) = 1 & (\Gamma) \\ \nabla\phi(x)\cdot\boldsymbol{n} = 0 & (\partial\Omega) \end{cases} \tag{5}$$

The boundary problem for the smeared interface can be expressed as:

$$\begin{cases} \alpha(\boldsymbol{x}) - \ell_\alpha^2\Delta\alpha(\boldsymbol{x}) = 0 & (\Omega) \\ \alpha(\boldsymbol{x}) = 1 & (\Gamma_\alpha) \\ \nabla\alpha(x)\cdot\boldsymbol{n} = 0 & (\partial\Omega) \end{cases} \tag{6}$$

B. Regularized Representation of Displacement Jump within the Interface

When a crack propagates into the interface between the aggregate and the matrix, it induces debonding phenomena. To accurately simulate this behavior, it is essential to integrate the cohesive law to describe the imperfect interface into the phase-field method. This model establishes a relationship between tractions $\boldsymbol{f}$ and displacement jumps $[\![\boldsymbol{u}]\!]$ along the interface through the following equation:

$$\boldsymbol{f} = \frac{\partial G([\![\boldsymbol{u}]\!],\mathcal{k})}{\partial[\![\boldsymbol{u}]\!]} \tag{7}$$

where $G([\![\boldsymbol{u}]\!],\mathcal{k})$ represents the fracture energy function, indicating the energy dissipation upon the creation of a unit crack surface, while $\mathcal{k}$ is the history parameter. In this cohesive fracture model, the energy is released gradually. Various cohesive laws exist in the literature, such as the Xu–Needleman

law and the bilinear law, which can be readily incorporated into the method. For this study, we adopt the Xu–Needleman law, defining tractions in the normal and shear directions as follows:

$$f_n = \frac{G_u}{\delta_n}\frac{[\![u_n]\!]}{\delta_n} exp\left(-\frac{[\![u_n]\!]}{\delta_n}\right) exp\left(-\frac{[\![u_s]\!]^2}{\delta_s^2}\right)$$

$$f_s = \frac{2G_u}{\delta_s}\frac{[\![u_s]\!]}{\delta_s}\left(1+\frac{[\![u_n]\!]}{\delta_n}\right) exp\left(-\frac{[\![u_n]\!]}{\delta_n}\right) exp\left(-\frac{[\![u_s]\!]^2}{\delta_s^2}\right) \quad (8)$$

where δ_n and δ_s represent the characteristic length parameters defined by $\delta_n = G_u/(f_u e)$ and $\delta_s = G_u/\left(f_u\sqrt{\frac{1}{2}}e\right)$ with $e = \exp(1)$, and f_u, and G_u represent the fracture strength and fracture toughness at the interface, respectively.

In a discrete formulation context, the crack opening at the interface is well-defined. However, within a regularization framework, both the crack and interface exhibit diffuse representations, leading to a similarly diffuse characterization of crack opening. Consequently, the displacement jump at Γ_α is replaced by an auxiliary jump field $\boldsymbol{\eta}$ defined as follows:

$$[\![\boldsymbol{u}]\!](\boldsymbol{x}) \approx \int_{-\infty}^{\infty} \boldsymbol{\eta}(\boldsymbol{x})\gamma(\alpha, \nabla\alpha)dx_n \quad (9)$$

where:

$$x_n = \left(\boldsymbol{x} - \boldsymbol{x}_{\Gamma_\alpha}\right)\cdot \boldsymbol{n}^{\Gamma_\alpha}$$

and

$$\boldsymbol{x}_{\Gamma_\alpha} = argmin_{\boldsymbol{y}\epsilon\Gamma_\alpha}(\|\boldsymbol{y}-\boldsymbol{x}\|)$$

This auxiliary jump field must satisfy the following condition, which means that this field constant in the normal direction of crack/interface:

$$\frac{\partial \boldsymbol{\eta}}{\partial x_n} = 0 \quad (10)$$

Therefore:

$$[\![\boldsymbol{u}]\!](\boldsymbol{x}) \approx \boldsymbol{\eta}(\boldsymbol{x}) \quad (11)$$

In order to define the interface between the aggregates and the cementitious matrix, the zero level set function $\varphi(\boldsymbol{x})$ proposed in [15] is used in this study. This function allows to define the interface with an arbitrary shape. It is defined as follows:

$$\begin{cases} \varphi(\boldsymbol{x}) > 0 \; for \; \boldsymbol{x} \in \Omega^i \\ \varphi(\boldsymbol{x}) < 0 \; for \; \boldsymbol{x} \in \Omega/\Omega^i \\ \varphi(\boldsymbol{x}) = 0 \; for \; \boldsymbol{x} \in \Gamma^I \end{cases} \quad (12)$$

where Ω^i denotes the set of aggregates, and Ω/Ω^i the matrix. Thus, the normal vector $\boldsymbol{n}^{\Gamma^\alpha}$ to the interface at point $\boldsymbol{x}$ is defined as follows:

$$\boldsymbol{n}^{\Gamma^\alpha} = \frac{\nabla\varphi(\boldsymbol{x})}{\|\nabla\varphi(\boldsymbol{x})\|} \quad (13)$$

It is noteworthty that, throughout the simulation, $\nabla\varphi(\boldsymbol{x})$ and $\boldsymbol{n}^{\Gamma^\alpha}$ remain constant because the interface does not evolve. i.e. it is determined only one at the beginning of the simulation.

C. A Phase-Field Model for Interfacial Cohesive Fracture

In this section, we develop a phase-field regularized zone model for interface modeling. We start by considering the potential energy of a cracked body with cohesive fracture, which is expressed as follows:

$$\mathbb{E} = \int_{\Omega/\Gamma} \Psi^e(\boldsymbol{u})d\Omega + \int_\Gamma g_c\, d\Gamma + \int_{\Gamma^I} G([\![\boldsymbol{u}]\!], \boldsymbol{\kappa})\, d\Gamma^I \quad (14)$$

where Ψ^e is the elastic energy density and g_c is the fracture energy of the bulk. Utilizing the smeared representation of crack, interface, and displacement jumps, we derive the regularized form of the energy

$$\mathbb{E} = \int_\Omega \left(g(\phi)\Psi^e(\boldsymbol{u},\boldsymbol{\eta}) + g_c\gamma_\phi(\phi,\nabla\phi) + G(\boldsymbol{\eta},\kappa)\gamma_\alpha(\alpha,\nabla\alpha) + \beta\frac{\partial\boldsymbol{\eta}}{\partial x_n}\cdot\frac{\partial\boldsymbol{\eta}}{\partial x_n}\right)d\Omega \quad (15)$$

The last term in (15) enforces the constant displacement jumps in the normal direction and β is the penalty parameter. The degradation function $g(\phi) = (1-\phi)^2 + \xi$ characterizes the loss of material strength, with ξ being very small and responsible for the stability of the solution. Subsequently, through the application of the principle of maximum dissipation and energy minimization, we derive a set of coupled equations for determining the phase field $\boldsymbol{\phi}(\boldsymbol{x})$, the displacement field $\boldsymbol{u}(\boldsymbol{x})$, and the displacement jump field $\boldsymbol{\eta}(\boldsymbol{x})$ as follows:

$$\begin{cases} 2(1-\phi)H - \frac{g_c}{\ell_\phi}\left(\phi - \ell_\phi^2\Delta\phi\right) = 0 & (\Omega) \\ \phi(\boldsymbol{x}) = 1 & (\Gamma) \\ \nabla\phi(\boldsymbol{x})\cdot\boldsymbol{n} = 0 & (\partial\Omega) \end{cases} \quad (16)$$

$$\begin{cases} \nabla\cdot\boldsymbol{\sigma}(\boldsymbol{u},\boldsymbol{\eta},\phi) = \boldsymbol{0} & (\Omega) \\ \boldsymbol{u}(\boldsymbol{x}) = \bar{u} & (\partial\Omega_u) \\ \boldsymbol{\sigma}\cdot\mathbf{n} = \bar{\boldsymbol{F}} & (\partial\Omega_F) \\ \gamma_\alpha(\boldsymbol{f}(\boldsymbol{\eta},\kappa) - \boldsymbol{\sigma}\cdot\mathbf{n}) = \beta\frac{\partial\boldsymbol{\eta}}{\partial x_n}\cdot\frac{\partial\boldsymbol{\eta}}{\partial x_n} & (\Gamma_\alpha) \\ \frac{\partial\eta(x_c)}{\partial x_n} = 0 & (\partial\Gamma_\alpha) \end{cases} \quad (17)$$

In (16), H is the history variable which is defined as follows:

$$H(\mathbf{x},t) = \max_{\tau\in[0,t]}\{\Psi^{e+}(\mathbf{x},t)\} \quad (18)$$

In (18), Ψ^{e+} represents the tensile part of the elastic strain density function. This part is utlized to describe the unilateral condition where the damage is due to traction. This function is defined as:

$$\Psi^{e+}(\boldsymbol{u},\boldsymbol{\eta}) = \frac{\lambda}{2}[\langle tr(\boldsymbol{\varepsilon}^e)\rangle_+]^2 + \mu tr\{(\boldsymbol{\varepsilon}^{e+})^2\} \quad (19)$$

where λ and μ are the Lamé constants. $\boldsymbol{\varepsilon}^e$ is the linearized strain tensor and $\langle x\rangle_\pm = (x \pm |x|)/2$ and $\boldsymbol{\varepsilon}^{e\pm}$ are the compression and tensile parts of the strain tensor. The elastic strain is defined as follows:

$$\boldsymbol{\varepsilon}^e = \nabla\boldsymbol{u} - \boldsymbol{n}^{\Gamma\alpha} \otimes^s \boldsymbol{\eta}\gamma_\alpha(\alpha,\nabla\alpha) \quad (20)$$

D. Finite Element Implementation

In this section, we detail the FEM discretizations to solve the damage and the displacement problem. The discretization of the phase field, the displacement field, and the displacement jumps field is expressed as follows:

$$\phi = \mathcal{N}_\phi \boldsymbol{\phi}^{el} \rightarrow \frac{\partial \phi}{\partial \boldsymbol{x}} = \mathcal{B}_\phi \boldsymbol{\phi}^{el} \quad (21)$$

$$\boldsymbol{u} = \mathcal{N}_{\boldsymbol{u}} \boldsymbol{u}^{el} \rightarrow sym\left(\frac{\partial u}{\partial \boldsymbol{x}}\right) = \mathcal{B}_u \boldsymbol{u}^{el}$$

$$\boldsymbol{\eta} = \mathcal{N}_{\boldsymbol{\eta}} \boldsymbol{\eta}^{el} \rightarrow sym(\boldsymbol{n}^{\Gamma_\alpha} \otimes^s \boldsymbol{\eta}) = \mathcal{B}_{\boldsymbol{\eta}} \boldsymbol{\eta}^{el},$$

$$\frac{\partial \boldsymbol{\eta}}{\partial x_n} = \mathcal{G}_{\boldsymbol{\eta}} \boldsymbol{\eta}^{el}$$

where $\mathcal{N}_\phi$, $\mathcal{N}_{\boldsymbol{u}}$, $\mathcal{N}_{\boldsymbol{\eta}}$ and $\mathcal{B}_\phi$, $\mathcal{B}_u$, $\mathcal{B}_{\boldsymbol{\eta}}$ are the vectors of the shape function and the matrix of the shape function derivatives of the phase field, displacement field, and displacement jumps field, respectively. $\boldsymbol{\phi}^{el}$, $\boldsymbol{u}^{el}$, $\boldsymbol{\eta}^{el}$ are the nodal values of ϕ, $\boldsymbol{u}$ and $\boldsymbol{\eta}$, respectively. With this discretization, firstly, we obtain the linear system of equations for the damage problem:

$$\mathcal{K}_\phi \boldsymbol{\phi} = \mathcal{K}_\phi \quad (22)$$

$$\mathcal{K}_\phi = \int_\Omega \left\{ \left(\frac{g_c}{\ell_\phi} + 2H_n \right) \mathcal{N}_\phi^T \mathcal{N}_\phi + g_c \ell_\phi \mathcal{B}_\phi^T \mathcal{B}_\phi \right\} \mathrm{d}\Omega \quad (23)$$

$$\mathcal{K}_\phi = \int_\Omega 2\mathcal{N}_\phi^T \, \mathrm{d}\Omega \quad (24)$$

Secondly, we obtain the nonlinear system of equations for the displacement field and the displacement jumps field as follows:

$$\mathcal{F}_{int,\boldsymbol{u}}(\boldsymbol{u}, \boldsymbol{\eta}) = \mathcal{F}_{ext,\boldsymbol{\eta}} \quad (25)$$

$$\mathcal{F}_{int,\boldsymbol{\eta}}(\boldsymbol{u}, \boldsymbol{\eta}) = 0$$

$$\mathcal{F}_{int,\boldsymbol{u}}(\boldsymbol{u}, \boldsymbol{\eta}) = \int_\Omega \left(\mathcal{B}_{\boldsymbol{u}}^T \mathbb{D} \mathcal{B}_{\boldsymbol{u}} \boldsymbol{u} - \gamma_\alpha \mathcal{B}_{\boldsymbol{u}}^T \mathbb{D} \mathcal{B}_{\boldsymbol{\eta}} \boldsymbol{\eta} \right) d\Omega \quad (26)$$

$$\mathcal{F}_{int,\boldsymbol{\eta}}(\boldsymbol{u}, \boldsymbol{\eta}) = \int_\Omega \left(-\gamma_\alpha \mathcal{B}_{\boldsymbol{\eta}}^T \mathbb{D} \mathcal{B}_{\boldsymbol{u}} \boldsymbol{u} + \gamma_\alpha^2 \mathcal{B}_{\boldsymbol{\eta}}^T \mathbb{D} \mathcal{B}_{\boldsymbol{\eta}} \boldsymbol{\eta} + \gamma_\alpha \mathcal{N}_{\boldsymbol{\eta}}^T \boldsymbol{f}(\boldsymbol{\eta}, \kappa) + \beta \mathcal{G}_{\boldsymbol{\eta}}^T \mathcal{G}_{\boldsymbol{\eta}} \right) d\Omega$$

Equation (25) is solved by a standard incremental Newton-Raphson procedure, utilizing the tangent stifness matrix:

$$\mathcal{K} = \begin{bmatrix} \mathcal{K}_{\boldsymbol{uu}} & \mathcal{K}_{\boldsymbol{u}\boldsymbol{\eta}} \\ \mathcal{K}_{\boldsymbol{\eta u}} & \mathcal{K}_{\boldsymbol{\eta\eta}} \end{bmatrix} \quad (27)$$

with:

$$\mathcal{K}_{\boldsymbol{uu}} = \int_\Omega (\mathcal{B}_{\boldsymbol{u}}^T \mathbb{D} \mathcal{B}_{\boldsymbol{u}}) d\Omega \quad (28)$$

$$\mathcal{K}_{\boldsymbol{u}\boldsymbol{\eta}} = \int_\Omega -\gamma_\alpha \mathcal{B}_{\boldsymbol{u}}^T \mathbb{D} \mathcal{B}_{\boldsymbol{\eta}} d\Omega$$

$$\mathcal{K}_{\boldsymbol{\eta u}} = \int_\Omega -\gamma_\alpha \mathcal{B}_{\boldsymbol{\eta}}^T \mathbb{D} \mathcal{B}_{\boldsymbol{u}} d\Omega$$

$$\mathcal{K}_{\boldsymbol{\eta\eta}} = \int_\Omega \left(\gamma_\alpha^2 \mathcal{B}_{\boldsymbol{\eta}}^T \mathbb{D} \mathcal{B}_{\boldsymbol{\eta}} + \gamma_\alpha \mathcal{N}_{\boldsymbol{\eta}}^T \frac{\partial f(\boldsymbol{\eta}, \kappa)}{\partial \boldsymbol{\eta}} \mathcal{N}_{\boldsymbol{\eta}} + \beta \mathcal{G}_{\boldsymbol{\eta}}^T \mathcal{G}_{\boldsymbol{\eta}} \right) d\Omega$$

where $\mathbb{D}$ is the elastic tensor.

III. RESULTS AND DISCUSSION

In this section, the influence of certain parameter of the phase -field model with imperfect interface is investigated. Assuming plain strain condition, we consider a square domain of 50 mm × 50 mm which contain two phases: aggregate and cementious matrix, along with the interface between them.

To characterize the heterogeneity of concrete, aggregates are individually placed within the cementitious matrix. The aggregates are assumed to have a circular shape, with diameters ranging from 15 to 4 mm. Each aggregate must adhere to two conditions: (i) it must be fully contained within the boundary of the concrete area and (ii) it must not overlap with any previously placed aggregates. The aggregate and cementitious mortar matrix are assumed to behave elastically. The proprieties of each phase are listed in Table I. The aggregate is assumed to be undamaged with its fracture energy being four times that of the mortar matrix.

TABLE I. MATERIAL PROPERTIES

Parameter	Aggregate	Mortar matrix
Young's modulus (MPa)	50	30.2
Poisson' ratio	0,21	0,21
Fracture energy (kN/mm)	4×10^{-6}	-

The 2D mesoscale of concrete, loading and boundary condition of the specimen are illustrated in Figure 2. The specimen is fixed at the bottom edge and subjected to a uniformly distributed displacemet at the top edge, i.e. a displacement-controlled loading scheme is used.

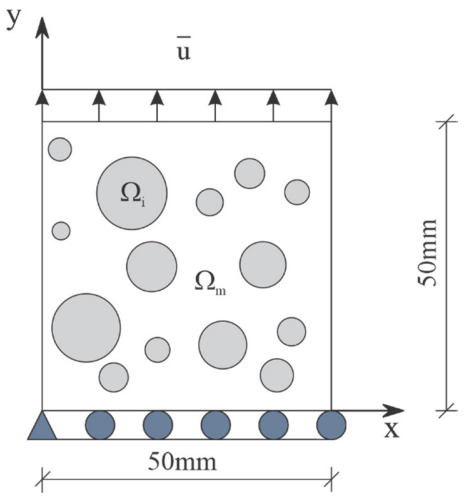

Fig. 2. 2D mesoscale of concrete, loading and boundary condition.

A. Influence of the Width of the Interface

In this section, we examine how the width of the interface affects the results. The internal length scale for crack ℓ_ϕ is set to 0.5 mm. Three different length scales for interface are analyzed: ℓ_α = 0.3, 0.5, and 1. In Figure 3, a smeared representation of the interface is shown for different values of the interface width. On the discrete interface α equals 1 and vanishes away from it. To meet the condition $\ell_\phi, \ell_\alpha \geq h_e$, the specimen is meshed with triangular elements, with the maximum mesh size set to 0.25 mm. The fracture strength is set to 1 MPa and the fracture energy of the interface is equals to half that of the matrix. The stress – displacement curves are

depicted in Figure 4. The crack path at peak stress and the crack pattern for different widths of interface are shown in Figure 5, in which, the blue color denotes the cementitious matrix, the green color represents the aggregate, and the red color denotes the crack. To better illustrate crack propagation, we highlight the crack area where $\phi > 0.9$. Depending on the width of the interface, the crack may occur either within the matrix or at the interface. More interfacial debonding occurs when $\ell_\alpha = 1$ than when $\ell_\alpha = 0.5$. Finally, the failure mode of all cases is characterized by a primary crack propagating perpendicular to the loading direction. However, the crack location of $\ell_\alpha = 0.3$ differs from the other cases and a slight difference between $\ell_\alpha = 1$ and $\ell_\alpha = 0.5$ is observed. It can be seen that as the width of the interface increases, the mode of crack changes from interfacial debonding to matrix cracking. The overall stress-displacement is also influenced by the width of the interface. As the width of the interface increases, both stiffness and peak stress of the specimen decrease and vice versa.

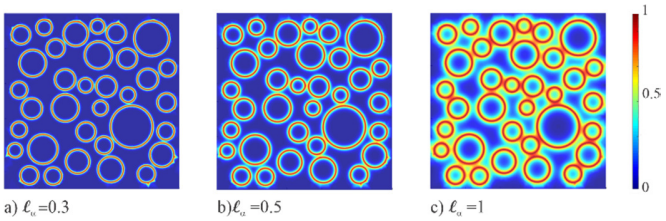

Fig. 3. Smeared representation of interface for different values of ℓ_α.

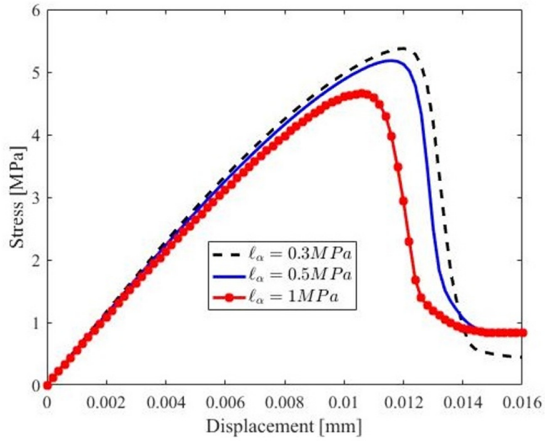

Fig. 4. Stress – displacement curve for different interface widths.

B. *Influence of Fracture Strength*

In this section, we investigate the influence of fracture strength f_u on the concrete crack behavior. Three fracture strength values are considered: 1, 5, and 10 MPa. The stress - displacement curves and obtained crack patterns are illustrated in Figures 6 and 7, respectively. The interface width is set to 0.5 mm and the fracture energy of interface remains half that of the matrix. Notably, when high strength interface is present, crack primarily initiates within the bulk of the material. A slight difference of the final crack pattern is noted between f_u = 5 MPa and f_u = 10 MPa. Notably, a higher fracture strength contributes to the increment of the specimen stiffness. However, only small differences in peak stress are observed between these cases. Moreover, the peak stress occurs earlier in the case of f_u = 10 MPa. Additionally, it is observed that interfaces with higher strength exhibit poorer post-cracking behavior.

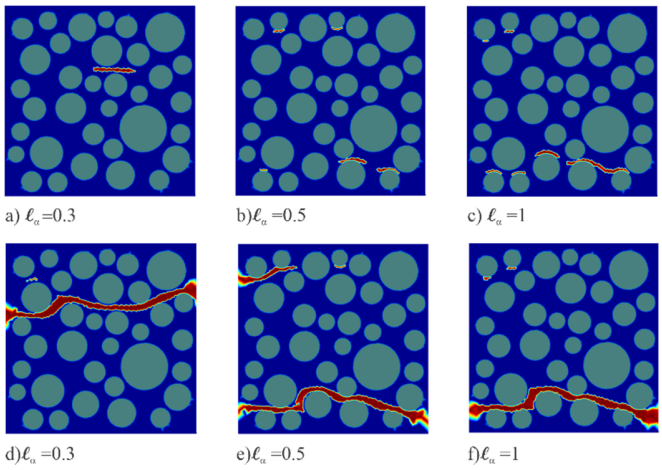

Fig. 5. Crack path and final crack pattern for difference interface widths.

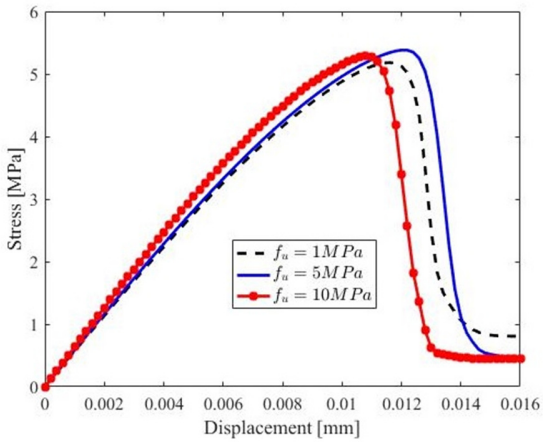

Fig. 6. Stress – displacement curve for different fracture strength f_u

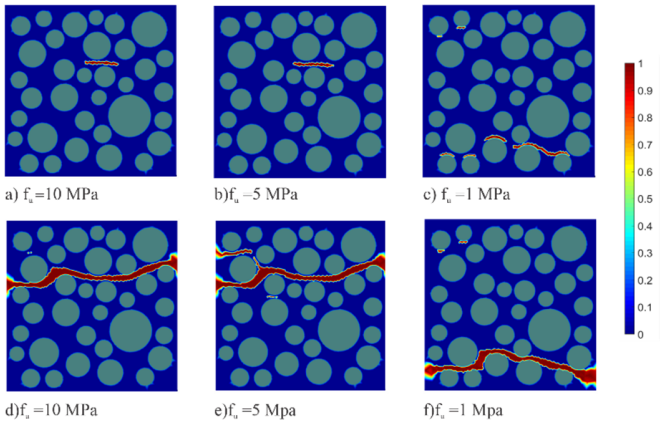

Fig. 7. Crack path and final crack pattern for different fracture strengths.

IV. CONCLUSION

This paper integrates the cohesive law to describe the imperfect interface into a phase field model to study crack propagation in concrete composites. We simulated a heterogeneous concrete specimen consisting of circular aggregates and cementitious material. The discrete interface location between the two materials is determined using the zero level set function. Subsequently, this discrete interface is smoothed out in a smeared manner using a fixed scalar variable. The displacement jump at the interface is modelled explicitly, using an auxiliary field, similar to a displacement field, over the entire domain. The effect of two parameters of models (the width of the interface and the fracture strength) on the crack patterns and stress – displacement curve is investigated. The main conclusions drawn from this study are:

- Increasing the width of the interface shifts the crack mode from interfacial debonding to matrix cracking. Consequently, both stiffness and peak stress of the specimen decrease with the widening of the interface. Moreover, variations in the width of the interface can lead to changes in the crack location.
- A switching from interfacial crack to bulk crack is observed when the fracture strength increases. The stronger interface properties can enhance the material stiffness. However, this could lead to a poorer post-cracking behavior.
- This phase field model with imperfect interface can be regarded as a valuable tool for investigating other types of concrete, such as steel fiber reinforced concrete, pervious concrete, and recycled aggregate concrete.

ACKNOWLEDGMENT

This research is funded by Ministry of Education and Training under Grand Number B2022-GHA-06.

REFERENCE

[1] H. Q. Nguyen, B. V. Tran, B. A. Le, and T. T. Nguyen, "On the choice of a phase field model for describing fracture behavior of concrete," *International Journal of Computational Materials Science and Engineering*, vol. 13, no. 01, Mar. 2024, Art. no. 2350016, https://doi.org/10.1142/S2047684123500161.

[2] H.-Q. Nguyen, B.-V. Tran, and T.-S. Vu, "Numerical approach to predict the flexural damage behavior of pervious concrete," *Case Studies in Construction Materials*, vol. 16, Jun. 2022, Art. no. e00946, https://doi.org/10.1016/j.cscm.2022.e00946.

[3] X. Li and Y. Xu, "Phase field modeling scheme with mesostructure for crack propagation in concrete composite," *International Journal of Solids and Structures*, vol. 234–235, Jan. 2022, Art. no. 111259, https://doi.org/10.1016/j.ijsolstr.2021.111259.

[4] W. Li and L. Guo, "Meso-fracture simulation of cracking process in concrete incorporating three-phase characteristics by peridynamic method," *Construction and Building Materials*, vol. 161, pp. 665–675, Feb. 2018, https://doi.org/10.1016/j.conbuildmat.2017.12.002.

[5] G. L. Peng and Y. H. Wang, "A Node Split Method for Crack Growth Problem," *Applied Mechanics and Materials*, vol. 182–183, pp. 1524–1528, 2012, https://doi.org/10.4028/www.scientific.net/AMM.182-183.1524.

[6] N. M. Azevedo and J. V. Lemos, "Hybrid discrete element/finite element method for fracture analysis," *Computer Methods in Applied Mechanics and Engineering*, vol. 195, no. 33–36, pp. 4579–4593, Jul. 2006, https://doi.org/10.1016/j.cma.2005.10.005.

[7] A. Boulenouar, N. Benseddiq, and M. Mazari, "Two-dimensional Numerical Estimation of Stress Intensity Factors and Crack Propagation in Linear Elastic Analysis," *Engineering, Technology & Applied Science Research*, vol. 3, no. 5, pp. 506–510, Oct. 2013, https://doi.org/10.48084/etasr.363.

[8] F. Zhou and J. F. Molinari, "Dynamic crack propagation with cohesive elements: a methodology to address mesh dependency," *International Journal for Numerical Methods in Engineering*, vol. 59, no. 1, pp. 1–24, Jan. 2004, https://doi.org/10.1002/nme.857.

[9] J. Y. Wu, J. Li, and R. Faria, "An energy release rate-based plastic-damage model for concrete," *International Journal of Solids and Structures*, vol. 43, no. 3–4, pp. 583–612, Feb. 2006, https://doi.org/10.1016/j.ijsolstr.2005.05.038.

[10] X. Q. Feng and S. W. Yu, "Damage Micromechanics for Constitutive Relations and Failure of Microcracked Quasi-Brittle Materials," *International Journal of Damage Mechanics*, vol. 19, no. 8, pp. 911–948, 2010, https://doi.org/10.1177/1056789509359662.

[11] C. Miehe, F. Welschinger, and M. Hofacker, "Thermodynamically consistent phase-field models of fracture: Variational principles and multi-field FE implementations," *International Journal for Numerical Methods in Engineering*, vol. 83, no. 10, pp. 1273–1311, Sep. 2010, https://doi.org/10.1002/nme.2861.

[12] N. Askarizadeh and M. R. Mohammadizadeh, "Numerical Analysis of Carbon Fiber Reinforced Plastic (CFRP) Shear Walls and Steel Strips under Cyclic Loads Using Finite Element Method," *Engineering, Technology & Applied Science Research*, vol. 7, no. 6, pp. 2147–2155, Dec. 2017, https://doi.org/10.48084/etasr.1279.

[13] V. A. Le and X. T. Nguyen, "The Effect of Cracks on the Free Vibration of a Plate with Parabolic Thickness," *Engineering, Technology & Applied Science Research*, vol. 13, no. 4, pp. 11100–11105, Aug. 2023, https://doi.org/10.48084/etasr.5923.

[14] J.-Y. Wu, "A unified phase-field theory for the mechanics of damage and quasi-brittle failure," *Journal of the Mechanics and Physics of Solids*, vol. 103, pp. 72–99, Jun. 2017, https://doi.org/10.1016/j.jmps.2017.03.015.

[15] T. T. Nguyen, J. Yvonnet, Q.-Z. Zhu, M. Bornert, and C. Chateau, "A phase field method to simulate crack nucleation and propagation in strongly heterogeneous materials from direct imaging of their microstructure," *Engineering Fracture Mechanics*, vol. 139, pp. 18–39, May 2015, https://doi.org/10.1016/j.engfracmech.2015.03.045.

[16] C. V. Verhoosel and R. De Borst, "A phase-field model for cohesive fracture," *International Journal for Numerical Methods in Engineering*, vol. 96, no. 1, pp. 43–62, Oct. 2013, https://doi.org/10.1002/nme.4553.

[17] K. Lê Gia, Q. Nguyễn Hoàng, and V. Trần Bảo, "Mô hình mặt tiếp xúc không hoàn hảo trong bê tông cốt sợi: bài toán một chiều," *Transport and Communications Science Journal*, vol. 74, no. 9, pp. 1063–1074, Dec. 2023, https://doi.org/10.47869/tcsj.74.9.4.